



First-Principles Study on the Impact of Stress on Depassivation of Defects at a -SiO₂/Si Interfaces

Xin Liu¹, Yang Liu^{2,3}, Hao-Ran Zhu¹, Xue-Hua Liu¹, Wen-Li Zhang¹ and Xu Zuo^{1,4,5*}

¹College of Electronic Information and Optical Engineering, Nankai University, Tianjin, China, ²Microsystem and Terahertz Research Center, China Academy of Engineering Physics, Chengdu, China, ³Institute of Electronic Engineering, China Academy of Engineering Physics, Mianyang, China, ⁴Key Laboratory of Photoelectronic Thin Film Devices and Technology of Tianjin, Nankai University, Tianjin, China, ⁵Engineering Research Center of Thin Film Optoelectronics Technology, Ministry of Education, Nankai University, Tianjin, China

OPEN ACCESS

Edited by:

Vincent G. Harris,
Northeastern University, United States

Reviewed by:

Yoshiyuki Miyamoto,
National Institute of Advanced
Industrial Science and Technology
(AIST), Japan
Xiao-Yong Fang,
Yanshan University, China

*Correspondence:

Xu Zuo
xzuo@nankai.edu.cn

Specialty section:

This article was submitted to
Quantum Materials,
a section of the journal
Frontiers in Materials

Received: 10 February 2022

Accepted: 07 April 2022

Published: 04 May 2022

Citation:

Liu X, Liu Y, Zhu H-R, Liu X-H, Zhang W-L and Zuo X (2022) First-Principles Study on the Impact of Stress on Depassivation of Defects at a -SiO₂/Si Interfaces.
Front. Mater. 9:872837.
doi: 10.3389/fmats.2022.872837

The amorphous silicon dioxide-silicon (a -SiO₂/Si) interface is an important part of silicon devices. It is difficult to avoid interface defects during the device production process. The passivated interface defects will undergo a depassivation reaction with the protons in the silicon dioxide generated by irradiation and convert to positively charged dangling bonds, thereby affecting device performance. In engineering practice, there is a final passivation layer on top of a -SiO₂, and it is inevitable to introduce stress on the a -SiO₂/Si interface. Therefore, studying the depassivation reaction mechanism of a -SiO₂/Si interface defects under stress is of great significance to understand the performance degeneration in real devices. By using molecular dynamics and first-principles calculations, P_b defects at a -SiO₂/Si (111) interface and P_{b1} defects at a -SiO₂/Si (100) interface are selected in this work to investigate the effect of stress on their depassivations. Biaxial strains are applied to the models, energy curves of the depassivation reactions under stress are calculated using the CI-NEB (Climbing Image Nudged Elastic Band) method, and transition states are identified. According to the Harmonic Transition State Theory (HTST), the reaction rate constants of the depassivation reactions of P_b and P_{b1} defects at a certain temperature can be obtained. Finally, the relative concentration curves during depassivation reactions of P_bH and $P_{b1}H$ under stress and room temperature are obtained. Detailed data and figure analyses are presented to demonstrate differences between the two typical interface defects when depassivating under stress. Appropriate degrees of interface stress are proved to extend the depassivation time of defects, therefore prolonging the service life of devices.

Keywords: first-principles calculation, depassivation, P_b -type defects, stress, a -SiO₂/Si interfaces

INTRODUCTION

As the key to integrated circuit technology, MOS structure is the core part of most silicon devices (Hughes and Benedetto, 2003). As an important part of MOS devices, the a -SiO₂/Si interface has a significant impact on the reliability of the device (Hughes and Benedetto, 2003). How to extend the service life of the device is an urgent problem to be solved. The main cause of device performance degradation is the existence of interface dangling bond defects. In the process of device fabrication, those defects are usually passivated by hydrogen and lose their electrical activity. However, when the

device is exposed to ionization radiation, the protons generated by the radiation will react with the passivated defects and convert them into positively charged dangling bonds, resulting in the degeneration of device performance (Rashkeev et al., 2001; Godet and Pasquarello, 2006; Li et al., 2018). Meanwhile, the radiation dose rate also impacts the degree of device ionization damage. Experiments showed that the ionization damage in a low-dose rate irradiation environment is more serious than that in a high-dose rate, which is called Enhanced Low-Dose-Rate Sensitivity (ELDRS) (Witczak et al., 2005; Pease et al., 2008; Chen, 2010). It was pointed out that the ELDRS effect is likely to be associated with the interface stress, and it is possible to relieve the ELDRS effect by removing the final passivation layer of the device (Shaneyfelt et al., 2002). Although the microscopic mechanisms behind the ELDRS effect is unknown at present, stress, as one of the known factors that affect ELDRS, should be paid special attention to in the selection of the final passivation layer materials and the encapsulation process of the device (Shaneyfelt et al., 2002; Boch et al., 2003; Shaneyfelt et al., 2003). Therefore, studying the influence of stress on the depassivation reactions of a -SiO₂/Si interface defects is highly valuable in reducing or even eliminating the ELDRS effect, improving the stability of the device, and extending the service life of the device in extreme environment.

Dangling bond defects at SiO₂/Si interfaces are usually called P_b -type defects. Experiments showed that all P_b -type defects share the same configuration [$-\text{Si}(\text{Si})_3$] and the same chemical properties. For example, P_b defects are all amphoteric (Lenahan, 2003). When the Fermi level is below the $+0$ charge state transition level, the defect will trap holes and is positively charged. The angle between the three backward Si-Si bonds becomes larger and the defect becomes an approximate planar structure, and this structure implies sp^2 hybridization in electronic structure. When the Fermi level is between the transition level $+0$ and $0/-$, the defect is electrically neutral. When the Fermi level is above the $0/-$ transition level, the defect will trap electrons and becomes negatively charged. The angle between the three backward Si-Si bonds becomes smaller, and the defect shows a stretched tetrahedral structure (Kovačević and Pivac, 2014). There are differences in their physical properties. P_b defects are located at the a -SiO₂/Si (111) interface, while P_{b0} and P_{b1} defects are located at the a -SiO₂/Si (100) interface. The dangling bonds of P_b and P_{b0} defects are along the [111] direction of crystalline silicon, while the P_{b1} dangling bond is roughly along the [211] direction (Stesmans et al., 1998). For the P_{b1} defect, there are three candidating configurations: dimer, bridge and AOD, among which the AOD configuration is more reasonable than the dimer and bridge configurations (Poindexter et al., 1981; Stesmans et al., 1998; Stirling et al., 2000; Stirling and Pasquarello, 2005).

The depassivation reaction process of P_b -type defects on the SiO₂/Si interface has been intensively investigated. Brower et al. showed that the depassivation reaction takes place in two steps. After a proton arrives at the interface, it first captures an electron and becomes an electrically neutral hydrogen atom, and then the hydrogen atom reacts with the passivated dangling bond: $P_b - \text{H} + \text{H} \rightarrow P_b + \text{H}_2$ (Stathis and Cartier, 1994; Godet and

Pasquarello, 2006) However, this proposition was questioned by Rashkeev et al. (2001), since only H^+ can be stable in SiO₂ and Si and diffuse to the interface. The study by Rashkeev et al. (2001) revealed that at the Si/SiO₂ interface, a proton can depassivate a Si dangling bond attached to an oxygen atom (i.e., the O-Si-H structure), and generate a positively charged Si dangling bond and a hydrogen molecule. This defect is also known as the Si₂O≡Si-defect and was intensively investigated previously (Mehes and Patterson, 2017). Based on the research above, it can be concluded that the passivated P_b -type defects can directly react with H^+ following the formula: $P_b - \text{H} + \text{H}^+ \rightarrow P_b^+ + \text{H}_2$. Later, this proposition was widely accepted.

In this work, by the first-principles calculation method based on Density Functional Theory (DFT), the reaction is simulated under different interface stresses. We choose the two most common P_b -type defects: P_b and P_{b1} (AOD), focus on the reaction processes of P_b and P_{b1} defects ($P_b\text{H}$ and $P_{b1}\text{H}$) being depassivated by protons to P_b^+ and P_{b1}^+ under stresses, and summarize the influence of stress on the depassivation reaction of P_b and P_{b1} defects. Following the viewpoint of Rashkeev et al., we simulate reactions that H^+ depassivates $P_b\text{H}$ or $P_{b1}\text{H}$ to generate a positively charged dangling bond: $P_b\text{H} + \text{H}^+ \rightarrow P_b^+ + \text{H}_2$, $P_{b1}\text{H} + \text{H}^+ \rightarrow P_{b1}^+ + \text{H}_2$. After constructing reasonable initial and final states, the depassivation reaction is simulated by the CI-NEB method. The activation energy and the pre-exponential factor of the transition state of one depassivation reaction can be quantitatively calculated, and then the depassivation reaction rate constant can be calculated. Curves of the relative concentrations of P_b and P_{b1} defects under different stresses during depassivation processes are plotted. For the P_b defect, the curves exhibit a scattered distribution over time, while those of the P_{b1} defect show a dense distribution. It also indicates that the depassivation reaction rate of the P_b defect is more likely to be greatly influenced by stress than that of the P_{b1} defect.

METHODS

First-Principles Calculation

The a -SiO₂/Si (100) and (111) interface models used in this work are derived from our previous works (Li et al., 2019a; Li et al., 2019b; Hong and Zuo, 2020). From a -SiO₂ and crystalline Si, the models are constructed through thermally oxidization of Si by a -SiO₂ using the Large-scale Atomic/Molecular Massively Parallel Simulator (LAMMPS) code (Plimpton, 1995; van Duin et al., 2001; van Duin et al., 2003; Fogarty et al., 2010). Passivation can improve the stability of the structure and properties, so it has important scientific significance and broad application prospects (Ya-Hui et al., 2020). In this manuscript, hydrogen is used to passivate dangling bond defects produced during interface thermal oxidation. Dimensions of the final a -SiO₂/Si (100) and (111) interface models are 15.5 Å × 15.5 Å × 35.0 Å and 13.3 Å × 15.4 Å × 49.4 Å, respectively. In the a -SiO₂/Si (100) interface model, the thicknesses of the seven-layer Si (100) moiety and a -SiO₂ moiety are 8.1 Å and 12.7 Å, respectively, with a vacuum

layer of 11.8 Å and a hydrogen passivation layer of 2.4 Å. In the *a*-SiO₂/Si (111) interface model, the thicknesses of the eight-layer Si (111) moiety and *a*-SiO₂ moiety are 10.2 Å and 15.1 Å, respectively, with a vacuum layer of 20.9 Å and a hydrogen passivation layer of 3.2 Å.

The first-principle calculations based on the Density Functional Theory are performed with the plane-wave basis, as implemented in the Vienna ab initio simulation package (VASP) (Kresse and Furthmüller, 1996). The electron core interaction is included by using the frozen-core all-electron projector augmented wave (PAW) method (Blöchl, 1994). The exchange correlation functional is treated by the generalized gradient approximation (GGA) parameterized by PERDEW, BURKE and ERNZERHOF (PBE) (Perdew et al., 1996). The plane-wave basis set cut-off energy is set as 520 eV for all calculations. Since the *a*-SiO₂/Si models are large in size, the Brillouin-zone integration is limited to the Γ point only. The structure is relaxed until the total energy is minimized. The convergence criterion of structural optimization is that the total energy difference is less than 10⁻⁵ eV, and the force on each atom is smaller than a tolerance of 0.05 eV/Å.

Harmonic Transition State Theory

Harmonic Transition State Theory (HTST) (Vineyard, 1957) is derived from a well-known theory—Transition State Theory (TST) (Henry, 1935; Voter and Doll, 1984). For many solid-state reactions, HTST is a good approximation as the energy barrier is usually larger than the average kinetic energy $k_B T$ in system. Another reason for using HTST as a reasonable approximation is that the harmonic approximation is often effective. Near the saddle point, the potential energy increases rapidly and forms a small bottleneck area. When using HTST, the first step is to find the saddle point corresponding to the reaction. There are many ways to find saddle points, and in this study we will use Climbing Image–Nudged Elastic Band (CI-NEB) method.

Climbing Image–Nudged Elastic Band

G. Henkelman developed the CI-NEB method to search for a transition state which is the first-order saddle point (Henkelman et al., 2000). The CI-NEB method specifically considers the problem of locating the transition state. The key difference between CI-NEB and Nudged Elastic Band (NEB) is the definition of the force on the point with the highest energy. In CI-NEB, this point will not be subjected to the spring force of the adjacent points, which can prevent its position from being pulled away from the transition state, therefore making this point climb to the transition state along the path in the direction of energy increase. The CI-NEB method requires only a few points, such as a total of five or even three points including the initial and final states to accurately locate the transition state. It is one of the most efficient methods to find a transition state. Between the initial and final structures of a reaction, appropriate number of images are inserted. In this work, the transition state and activation energy of the P_b-type defect depassivation reaction are obtained by the CI-NEB method.

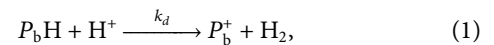
Applying Strains

In order to simulate the stress induced by the final passivation layer, a biaxial strain is applied at the *a*-SiO₂/Si (111) and (100) interfaces (Zhou et al., 2014; Grote and Berger, 2015; Al-Shami et al., 2018). The biaxial strain is imposed on the relaxed unit cell along *x*-axis and *y*-axis ([100] and [010] direction) according to the equations (Al-Shami et al., 2018): $\epsilon_a(\%) = (a - a_0)/a_0$; $\epsilon_b(\%) = (b - b_0)/b_0$, where ϵ_a and ϵ_b represent strain degrees of the model in *x* and *y* direction, *a* and *a*₀ are the strained and original lattice constants in *x* direction, and *b* and *b*₀ are the strained and original lattice constants in *y* direction. We successively change the lattice constants *a* and *b* and relax models to simulate the effect of stress on the interfaces.

KINETICS OF P_B AND P_{B1} DEPASSIVATIONS

Taking the P_b defect at *a*-SiO₂/Si (111) interface as an example, the concentration ratio of depassivated defects and passivated defects in an initial condition is deduced. Derived formulas are also applicable to the P_{b1} defect at *a*-SiO₂/Si (100) interface.

From the above introduction, the reaction of P_bH depassivated by H⁺ is:



where k_d is the depassivation reaction rate constant. According to the chemical reaction kinetic theory (HSteinfeld et al., 1999), the reaction rate equation can be written as:

$$d[P_b^+]/dt = k_d [P_bH] [H^+], \quad (2)$$

where $[P_b^+]$ is the concentration of P_b⁺, $[P_bH]$ is the concentration of P_bH, and $[H^+]$ is the concentration of H⁺, which depends on its diffusion. Eq. 2 can also be written as:

$$d[P_b^+]/dt = k_d (N_0 - [P_b^+]) [H^+], \quad (3)$$

where N_0 is the total density of the P_bH center in the initial condition. Set $[P_b^+]/N_0 = x$, *x* is the relative concentration of P_b⁺ defects. Then Eq. 3 can be written as:

$$dx/dt = k_d [H^+] (1 - x), \quad (4)$$

The solution of the above first-order differential equation is:

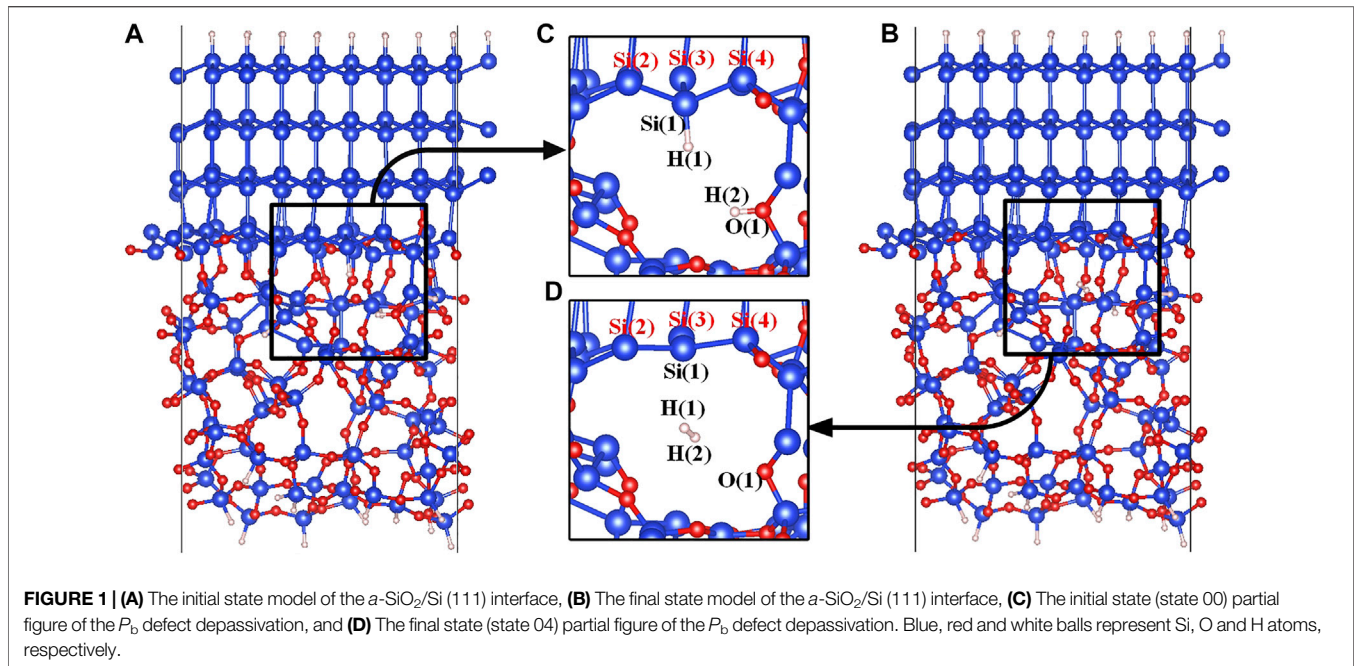
$$x = 1 - \exp(-k_d [H^+] t), \quad (5)$$

where *t* is time. The above approximation holds for the slow depassivation at a low proton concentration.

Therefore, the key to solving the relative concentration *x* of interface defects P_b⁺ and P_{b1}⁺ during the depassivation reaction is to solve the reaction rate constant k_d . From the Arrhenius equation, we can write the depassivation reaction rate constants k_d and k_{ds} (Brower and Myers, 1990) as follows,

$$k_d = k_{d0} \exp[-E_d / (k_B T)], \quad (6)$$

$$k_{ds} = k_{ds0} \exp[-E_{ds} / (k_B T)], \quad (7)$$



where E_d is the activation energy of the depassivation reaction without stress, and E_{ds} is the activation energy of the depassivation reaction under stress. k_{dso} and k_{d0} are the pre-exponential factors for the depassivation reaction with and without stress, respectively. k_B is Boltzmann's constant equal to 1.38×10^{-23} J/K, T is temperature (unit: K), and the relevant reduction unit of Boltzmann's constant $k_B T$ is 25.852 meV ($T = 300$ K).

According to the Harmonic Transition State Theory (HTST), the activation energy and transition state can be calculated by the CI-NEB method, and then the reaction rate can be calculated by the following equation:

$$k_{HTST} = \frac{\prod_i^{3N} \nu_i^R}{\prod_i^{3N-1} \nu_i^S} \exp[-(E^S - E^R)/(k_B T)], \quad (8)$$

where N is the number of atoms, ν_i^R and E^R are the stable vibration frequencies of the reactant and the energy respectively in the initial state, and ν_i^S and E^S are the real vibration frequencies and the energy respectively in the transition state. The function form of HTST is analogous to the empirically derived Arrhenius rate Eqs 6, 7. The pre-exponential factor in the Arrhenius rate law is given by the ratio of the product of real atomic vibrational frequencies at the initial state over that at the saddle point in HTST (Vineyard, 1957).

RESULTS AND DISCUSSION

Depassivation of the P_b Defect Without Stress

Structures of the P_b defect are shown in Figures 1C,D. Si(1) is the defective atom, and the three silicon atoms bonded with

TABLE 1 | Three Si-Si-Si bond angles and the parameter t .

	$\angle \text{Si}(2)\text{-Si}(1)\text{-Si}(3)$ (°)	$\angle \text{Si}(3)\text{-Si}(1)\text{-Si}(4)$ (°)	$\angle \text{Si}(4)\text{-Si}(1)\text{-Si}(2)$ (°)	t
P_b	102.17	100.78	120.93	1.15
P_b^*	112.71	107.31	137.13	0.09

Si(1) are directly connected to the crystalline silicon moiety through Si-Si bonds. In order to simulate the depassivation reaction of the P_b defect at the a -SiO₂/Si (111) interface, the initial and final states of the reaction need to be constructed first. In the initial state of the reaction, the defective atom Si(1) is passivated with the atom H(1), and the proton H(2) is stably connected to the Si-O(1)-Si bridge (Yue et al., 2018). In the final state of the reaction, a hydrogen molecule is formed in the void near the defect. It is worth mentioning that before carrying out further calculations, the stability of the initial and final state structures needs to be confirmed (Pei et al., 2021; Ying-Ying et al., 2021). The atomic vibrational frequencies of initial and final state structures must be calculated first to make sure that there is no imaginary frequency. It is based on this operation that the reaction processes can be simulated correctly in this manuscript. The initial and final states of the P_b defect depassivation reaction are shown in Figure 1.

Since the P_b defect generated by the depassivation is positively charged, the defective Si atom and the surrounding three silicon atoms form a nearly planar structure in the final state, as shown in Figure 1D. The tetrahedral distortion parameter t is defined as $t = (360 - \sum_{i=1,3} \alpha_i)/31.5$ where $\sum_{i=1,3} \alpha_i$ is the sum of three bond angles (Blöchl, 2000). In this manuscript t is used to measure the hybridization of the defective silicon atom. For an sp^3 hybridized silicon atom with a perfect tetrahedral structure, t is one, whereas

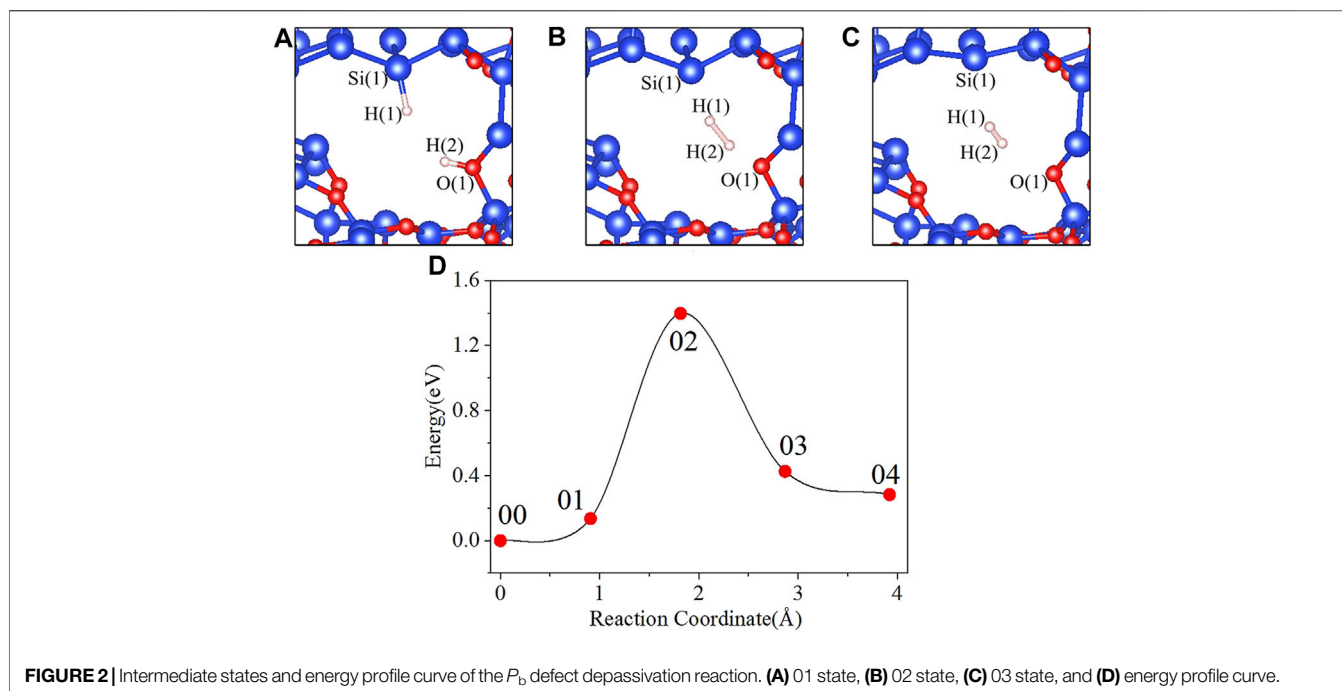


FIGURE 2 | Intermediate states and energy profile curve of the P_b defect depassivation reaction. (A) 01 state, (B) 02 state, (C) 03 state, and (D) energy profile curve.

TABLE 2 | H-H, Si-H and O-H bond lengths, and the energies of the states in P_b depassivation reaction.

	00	01	02	03	04
H(1)-H(2)	2.857	2.269	1.100	0.763	0.755
Si(1)-H(1)	1.508	1.531	1.889	2.470	2.783
O(1)-H(2)	0.984	0.986	1.323	2.102	2.728
Energy (eV)	0.000	0.135	1.398	0.426	0.283

for an sp^2 hybridized silicon atom with a planar trigonal structure, t is zero (Blöchl, 2000). The comparisons between the P_b defect and the P_b^+ defect on three Si-Si-Si bond angles and the parameter t are listed in **Table 1**. It can be seen from **Table 1** that the t parameter of the P_b defect is 1.15 when it is neutral, and the defect atom is close to an ideal sp^3 hybridization. When the P_b defect is positively charged as P_b^+ , the t parameter is 0.09, and the defect atom is close to an ideal sp^2 hybridization.

In the initial state 00 of the depassivation reaction, the bond lengths of Si(1)-H(1) and O(1)-H(2) are 1.508 and 0.984 Å, respectively, and the distance between H(1) and H(2) is 2.857 Å. From the initial state 00 to the state 02, H(1) and H(2) tend to move towards each other, and the lengths of Si(1)-H(1) and O(1)-H(2) bonds keep increasing until the bonds are broken. When the reaction proceeds to the transition state 02, the energy of the system reaches a highest point of 1.398 eV. In the 02 state, the distances between Si(1) and H(1), O(1) and H(2), and H(1) and H(2) are 1.889, 1.323, and 1.100 Å, respectively. As the reaction proceeds from state 02 to state 04, the distance between H(1) and H(2) is decreasing, while the distances between Si(1) and H(1), and O(1) and H(2) keep increasing. In the final state 04, the H(1)-H(2) bond length stabilizes at a value of 0.755 Å. The three intermediate states and the energy profile curve are

shown in **Figure 2**. The bond lengths and energies of the states during the depassivation reaction are listed in **Table 2**.

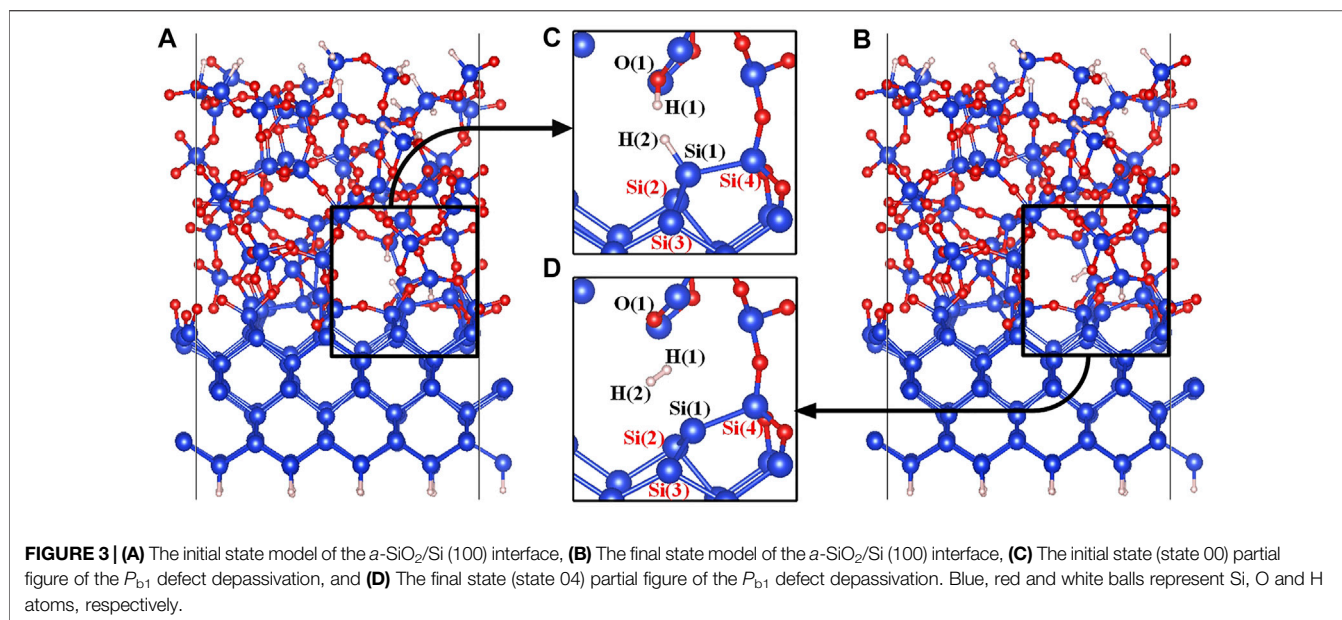
It can be extracted from **Figure 2D** that the 02 state is the transition state and the activation energy is 1.398 eV. VASP is hired to calculate the vibration frequencies. There is no imaginary frequency in the initial and final states, and there is one and only one in the transition state. The calculated pre-exponential factor is $1.44 \times 10^{-7} \text{ cm}^3 \text{ s}^{-1}$.

Depassivation of the P_{b1} (AOD) Defect Without Stress

Structures of the P_{b1} (AOD) defect are shown in **Figures 3C,D**. Si(1) is the defective atom, and Si(4) as one of the three silicon atoms connected to Si(1), is linked to the α -SiO₂ moiety through one Si-O-Si bridge and to the crystalline silicon moiety through two Si-O-Si bridges. In the initial state of the P_{b1} (AOD) defect depassivation, the proton H(1) is stably connected to the Si-O(1)-Si bridge to form the O(1)-H(1) bond (Yue et al., 2018), and the atom H(2) is chosen to passivate the defective atom Si(1). In the final state, a hydrogen molecule is formed in the void near the P_{b1}^+ defect. The initial and final state diagrams are shown in **Figure 3**.

It can be seen from the final state partial **Figure 3D** that the defective silicon atom Si(1) and the surrounding three atoms form a plane-like structure. The comparisons between the P_{b1} defect and the P_{b1}^+ defect on three Si-Si-Si bond angles and the parameter t are listed in **Table 3**. When the P_{b1} defect is neutral, the t parameter is 1.25 close to the value of one for a perfectly sp^3 hybridized atom. For the positively charged P_{b1}^+ defect, the t value is 0.41 close to the perfect sp^2 hybridization value zero.

In the initial state 00, the bond lengths of Si(1)-H(2) and O(1)-H(1) are 1.501 Å and 0.989 Å, respectively, and the distance

**TABLE 3 |** Three Si-Si-Si bond angles and the parameter t .

	$\angle\text{Si}(2)\text{-Si}(1)\text{-Si}(3)$ ($^\circ$)	$\angle\text{Si}(3)\text{-Si}(1)\text{-Si}(4)$ ($^\circ$)	$\angle\text{Si}(4)\text{-Si}(1)\text{-Si}(2)$ ($^\circ$)	t
P_{b1}	102.21	117.57	100.99	1.25
P_{b1}^+	112.27	128.39	106.27	0.41

between H(1) and H(2) is 2.665 Å. From the initial state 00 to the intermediate state 01, H(1) gradually separates from O(1), and H(2) gradually separates from Si(1). When the reaction proceeds to the 02 state, the system energy reaches the maximum value of 0.931 eV. In the 02 state, the distances between Si(1) and H(2), O(1) and H(1), and H(1) and H(2) are 1.758, 1.353, and 1.035 Å, respectively. As the reaction progresses, the distance between Si(1) and H(2) keeps increasing, and the distance between O(1) and H(1) is also gradually increasing while the distance between H(1) and H(2) is gradually decreasing. Finally the reaction proceeds to the final state 05, where the H(1)-H(2) bond length is 0.740 Å. The four intermediate states diagrams and the energy profile curve are shown in **Figure 4**. The bond lengths and energies of the states during the depassivation reaction are listed in **Table 4**.

In **Figure 4E**, the 02 state is the transition state, and the activation energy is 0.931 eV. VASP is used to calculate the vibration frequencies and there is no imaginary frequency in the initial and final states, and one and only one in the transition state. The calculated pre-exponential factor is $2.71 \times 10^{-8} \text{ cm}^3 \text{ s}^{-1}$.

Apply Stress to $a\text{-SiO}_2/\text{Si}$ (111) and (100) Interfaces

In order to simulate the stress induced by the final passivation layer, a biaxial strain is applied to the $a\text{-SiO}_2/\text{Si}$ (111) and (100) interfaces, and the strain degree ϵ ranges from -7% to 7% with a

step of 1%. The stress-strain scatter diagrams are shown in **Figure 5**. The external pressure is the equivalent pressure on the interface after stress is applied. A positive value indicates that the interface is compressed, and a negative value indicates that the interface is stretched. It is shown by the figure that the external pressure (or its absolute value) is almost linearly proportional to the strain degree.

In addition to the stress-strain curves, the change of average bond length and average bond angle also reflects the degree of deformation of models to a certain extent. In order to facilitate a more detailed analysis of the structural properties of models, and to further verify the rationality of the stress applied, a statistical analysis of the bond lengths and bond angles is conducted, including the average values and the increase rates. The increase rate is defined as the ratio of the increase value of bond length (or bond angle) in a certain stage to the initial value. **Tables 5, 6**, respectively show the average lengths of Si-O bond in $a\text{-SiO}_2$ part and Si-Si bond in crystalline silicon part, and the average angles of $\angle\text{O-Si-O}$ and $\angle\text{Si-O-Si}$ in $a\text{-SiO}_2$ part with strains of -7% , 0% and 7% .

It is shown by the above two tables that, as the strain degree ϵ of the $a\text{-SiO}_2/\text{Si}$ interface increases from -7% to 7% , the average values of bond lengths and bond angles also increase. However, the increase rate γ is different. When ϵ increases in a certain extent, i.e., from -7% to 0% or from 0% to 7% , the Si-Si bond exhibits a higher average increase rate of 2.65%, while that of the Si-O bond is 0.45%. It can be concluded that the Si-Si bond is

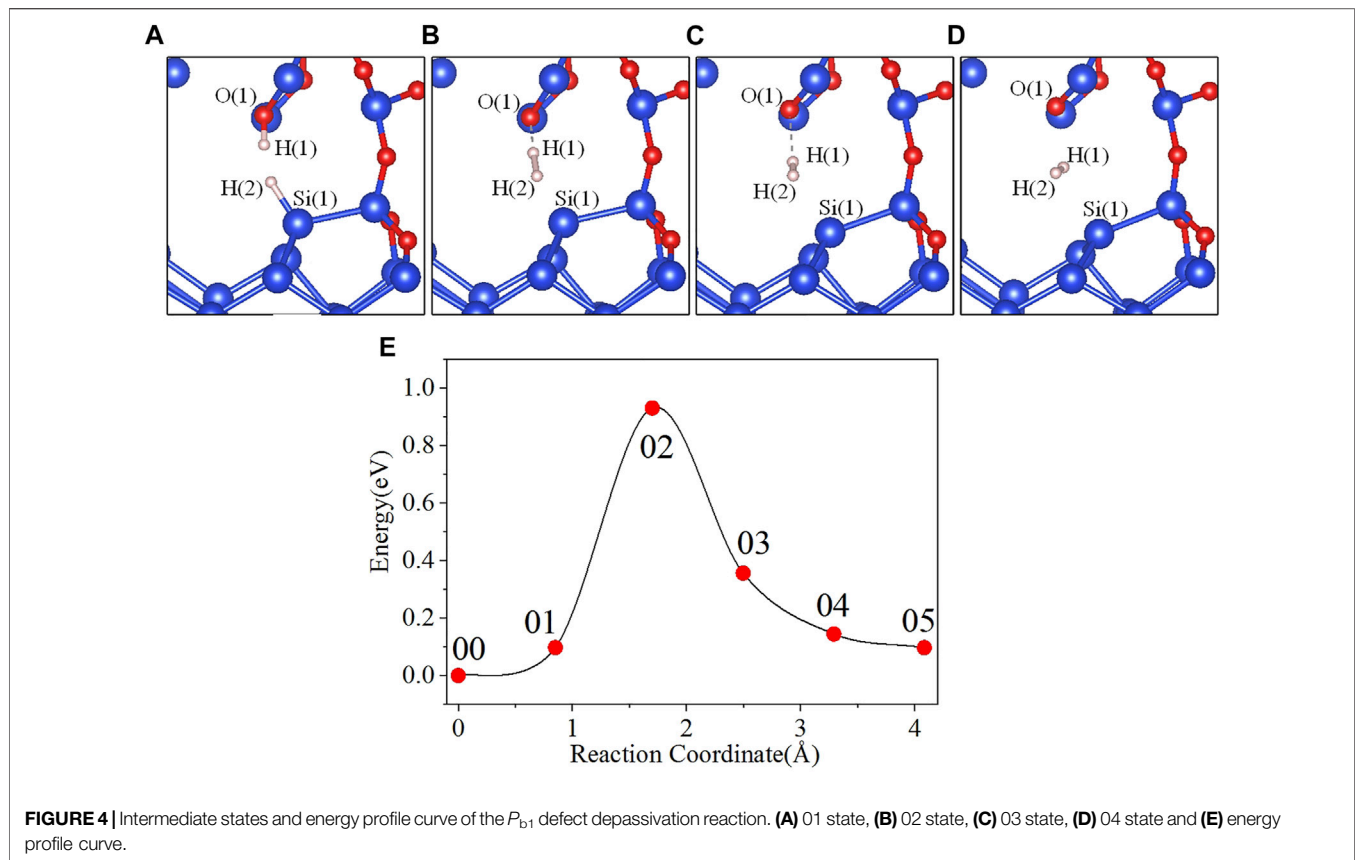


TABLE 4 | H-H, Si-H and O-H bond lengths and the energies of the states in P_{b1} depassivation reaction.

	00	01	02	03	04	05
H (1)-H (2)	2.665	2.083	1.035	0.773	0.763	0.740
Si(1)-H (2)	1.501	1.516	1.758	2.133	2.315	2.312
O (1)-H (1)	0.989	0.995	1.353	2.039	2.567	3.049
Energy (eV)	0	0.097	0.931	0.357	0.145	0.097

relatively more sensitive to stress. For the bond angles, $\angle\text{Si-O-Si}$ has an average increase rate of 2.68% while $\angle\text{O-Si-O}$ has an average increase rate of 0.10%. It can be seen that compared to $\angle\text{O-Si-O}$, $\angle\text{Si-O-Si}$ is more sensitive to stress.

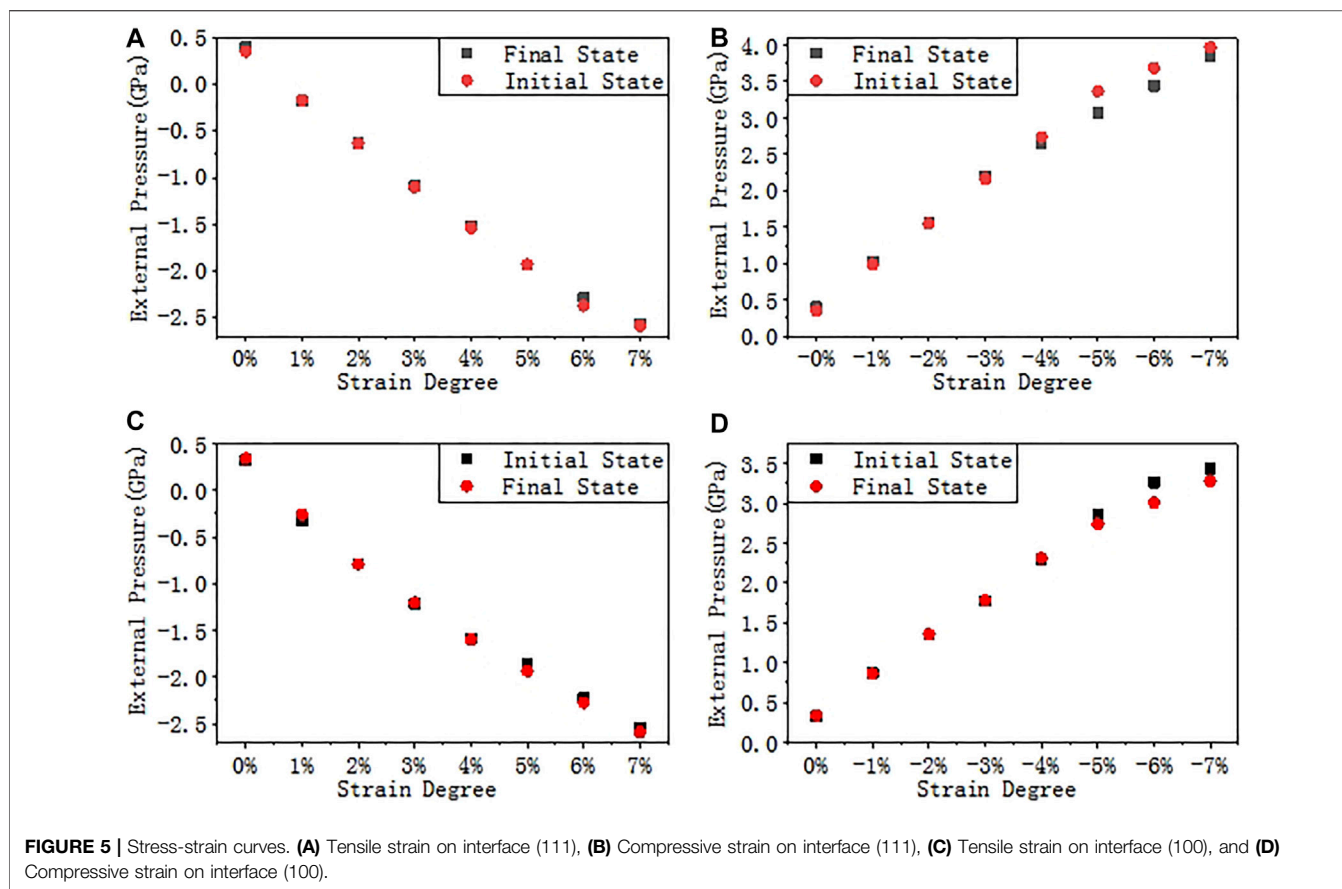
Depassivations of P_b and P_{b1} Defects Under Stress

After applying stress to the interface models, the depassivation reactions of the interface defects under different stresses are investigated. Tensile and compressive strains are applied to the $\alpha\text{-SiO}_2/\text{Si}$ (111) and (100) interfaces and the activation energies of P_b and P_{b1} defects depassivations under different strains are listed in **Tables 7, 8**. The energy curves during depassivation reactions and activation energy profile curves (**Figures 6–9**) under different stresses are shown below.

From **Figure 6** and **Table 7**, it can be concluded that when the tensile strain degree ε is between 0% and 4%, the activation energy of P_b defect depassivation reaction is stable at about 1.35 eV, and the fluctuation range is less than 0.07 eV. When the strain degree ε increases from 4% to 5%, the activation energy surges by 0.76–2.05 eV. Afterwards as the strain degree ε increases, the activation energy stabilizes at a higher value of about 2.00 eV.

In **Figure 7** and **Table 7**, as the strain degree ε decreases from 0% to –3%, the P_b depassivation reaction activation energy stabilizes at about 1.40 eV, and the fluctuation is less than 0.07 eV. Within this strain range, the forward reaction barrier of the depassivation reaction is always higher than the reverse one. When the strain degree ε decreases from –3% to –4%, the activation energy drops drastically to 1.17 eV, and the forward reaction barrier becomes smaller than the reverse reaction barrier. Then, as the strain degree ε decreases from –4% to –7%, the reaction activation energy also gradually decreases and is less than 1 eV, and the forward reaction barrier of the reaction is always smaller than the reverse one.

In **Figure 8** and **Table 8**, as the tensile strain degree ε increases, the activation energy of the P_{b1} defect depassivation reaction does not change much. It is basically stable at about 0.90 eV and the fluctuation is less than 0.08 eV. From the depassivation reaction curves, when ε increases to 6%, the reverse reaction barrier of the depassivation reaction becomes higher than the forward reaction barrier.

**TABLE 5 |** The average lengths and increase rates of Si-O bond and Si-Si bond at different strains.

Strain degree ϵ		<i>a</i> -SiO ₂ /Si (111) interface			<i>a</i> -SiO ₂ /Si (100) interface		
		-7%	0%	7%	-7%	0%	7%
Si-O bond	Length (Å)	1.636	1.641	1.650	1.638	1.643	1.653
	Increase rate		0.31%	0.55%		0.31%	0.61%
Si-Si bond	Length (Å)	2.291	2.355	2.429	2.311	2.360	2.420
	Increase rate		2.79%	3.14%		2.12%	2.54%

TABLE 6 | The average angles and increase rates of \angle O-Si-O and \angle Si-O-Si at different strains.

Strain degree ϵ		<i>a</i> -SiO ₂ /Si (111) interface			<i>a</i> -SiO ₂ /Si (100) interface		
		-7%	0%	7%	-7%	0%	7%
\angle Si-O-Si	Angle (°)	135.675	139.766	142.637	134.126	137.930	141.819
	Increase rate		3.02%	2.05%		2.84%	2.82%
\angle O-Si-O	Angle (°)	109.215	109.378	109.502	109.310	109.355	109.445
	Increase rate		0.15%	0.11%		0.04%	0.08%

In **Figure 9** and **Table 8**, the activation energy of the depassivation reaction of P_{b1} defects is stable at about 0.92 eV under compressive strain, and the fluctuation is less than 0.07 eV. As the degree of compressive strain increases, the reverse reaction barrier becomes higher than the forward one.

Calculation of the Relative Concentrations of P_b and P_{b1} Defects

According to **Eq. 8**, as long as the activation energy and the pre-exponential factor are obtained, the reaction rate k_d can be solved for a chemical reaction. The pre-exponential factor is the ratio of

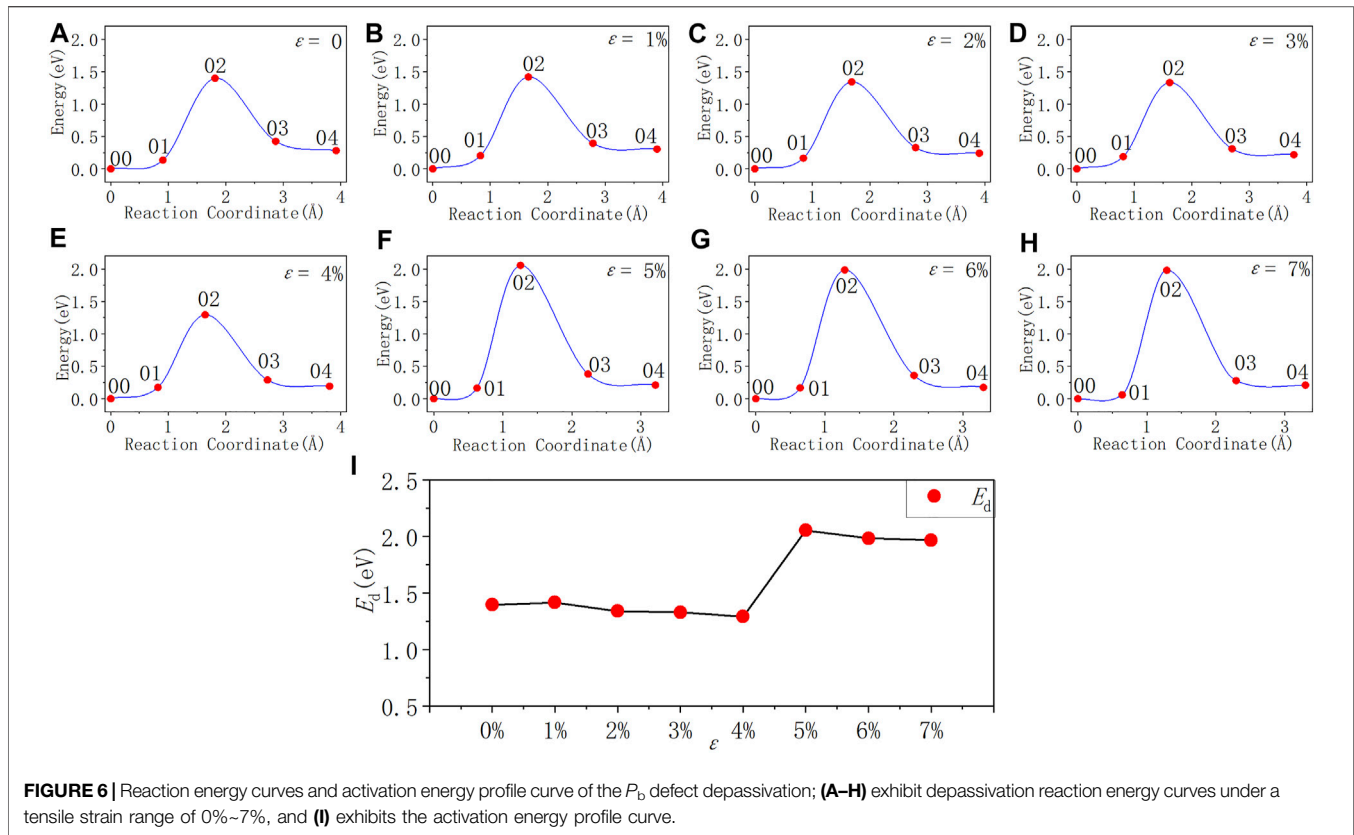


TABLE 7 | Activation energies of P_b defect depassivations under tensile and compressive strains.

ε	0%	1%	2%	3%	4%	5%	6%	7%
E_d (eV)	1.398	1.417	1.341	1.331	1.293	2.055	1.984	1.969
ε	0%	-1%	-2%	-3%	-4%	-5%	-6%	-7%
E_d (eV)	1.398	1.449	1.465	1.458	1.173	0.943	0.783	0.743

TABLE 8 | Activation energies of P_{b1} defect depassivations under tensile and compressive strains.

ε	0%	1%	2%	3%	4%	5%	6%	7%
E_d (eV)	0.931	0.862	0.891	0.912	0.936	0.920	0.955	0.971
ε	0%	-1%	-2%	-3%	-4%	-5%	-6%	-7%
E_d (eV)	0.931	0.897	0.858	0.985	0.956	0.908	0.922	0.933

the product of the vibration frequencies of the initial state and the product of all real vibration frequencies of the transition state of the reaction. In this study, VASP code is used to calculate pre-exponential factors of different depassivation reactions. Combined with the reaction activation energy shown in the previous part, the depassivation reaction rates of P_b and P_{b1} defects under different strain degrees at room temperature (300K) are calculated. The results are exhibited in **Tables 9, 10** and curves are plotted in **Figure 10**.

It can be seen that at room temperature the depassivation reaction rate of P_{b1} defects is generally faster than that of P_b defects. For P_b defects, when the strain degree ε is 5%, the depassivation reaction rate is the slowest; when ε is -7%, the depassivation reaction rate is the fastest. In addition, when the strain degree ε is in the range of -7%~ -5%, the depassivation reaction rate is relatively fast, which is 8–11 orders of magnitude faster than that without stress; when ε is in the range of 5%–7%, the depassivation reaction rate is relatively slow, which is 10–12 orders of magnitude slower than that in the case of no stress. For P_{b1} defects, the depassivation reaction rate changes generally steady, and there is no significant increase or decrease as stress is applied. When the strain degree $\varepsilon = -2\%$, the depassivation reaction rate is the fastest, which is two orders of magnitude faster than that without stress. The increase or decrease of depassivation rate under other strain degrees is insignificant. It can be inferred that the depassivation of P_{b1} defects on the a -SiO₂/Si (100) interface is insusceptible of stress, while the depassivation of P_b defects on the a -SiO₂/Si (111) interface can be greatly affected by stress.

After obtaining the depassivation reaction rate constant k_d , the curve of the relative concentration value (x) of the defect with time (t) can be calculated according to **Eq. 5**. Researchers have studied the hydrogen/deuterium diffusion in solid-state crystallized (SSC) poly-Si and low-pressure chemical-vapor-deposited (LPCVD)-grown polycrystalline silicon. The study pointed out that the H surface concentration amounts to $\approx 10^{19}$ and $\approx 3 \times 10^{19}$ cm⁻³ in LPCVD-grown and SSC poly-Si,

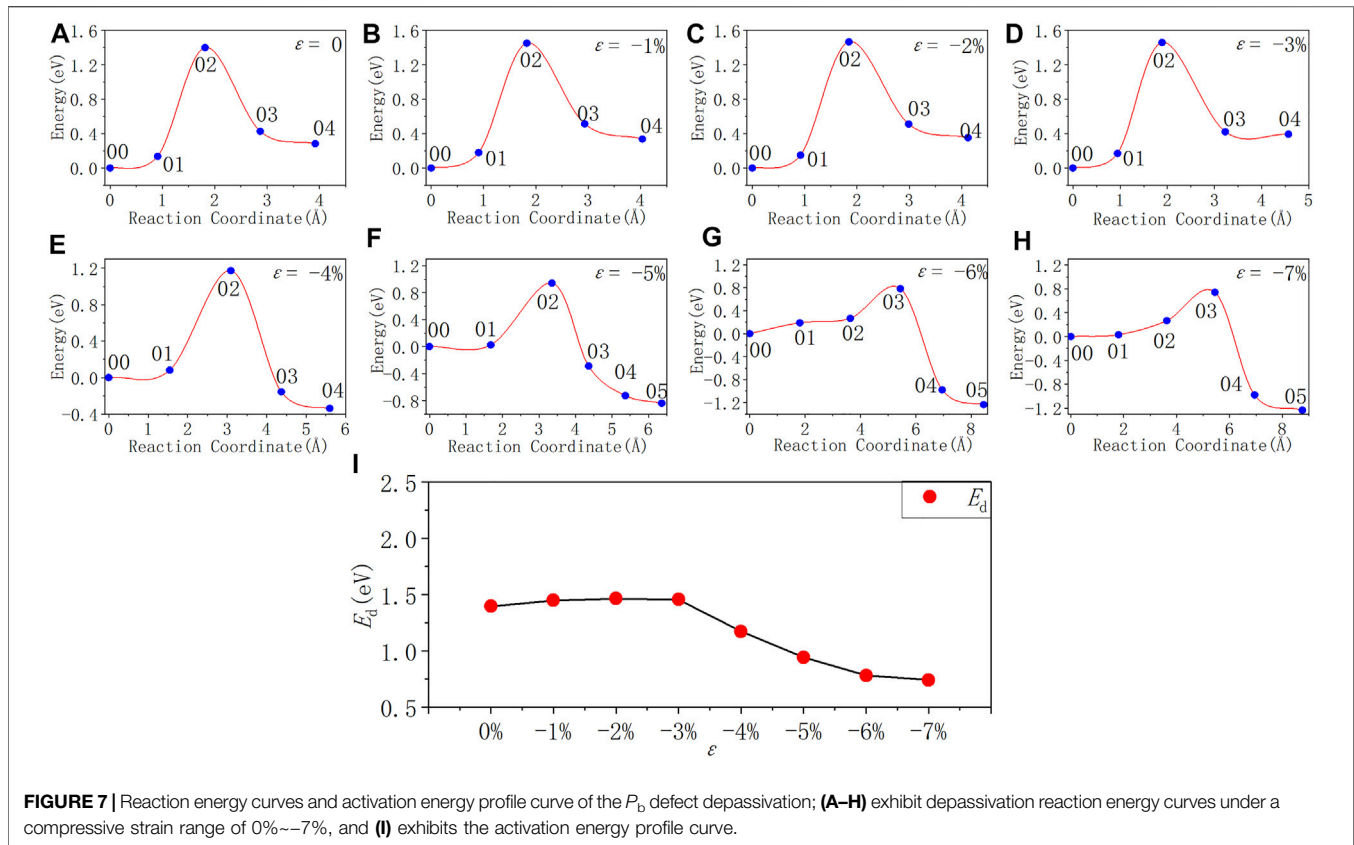


FIGURE 7 | Reaction energy curves and activation energy profile curve of the P_b defect depassivation; (A–H) exhibit depassivation reaction energy curves under a compressive strain range of 0%–7%, and (I) exhibits the activation energy profile curve.

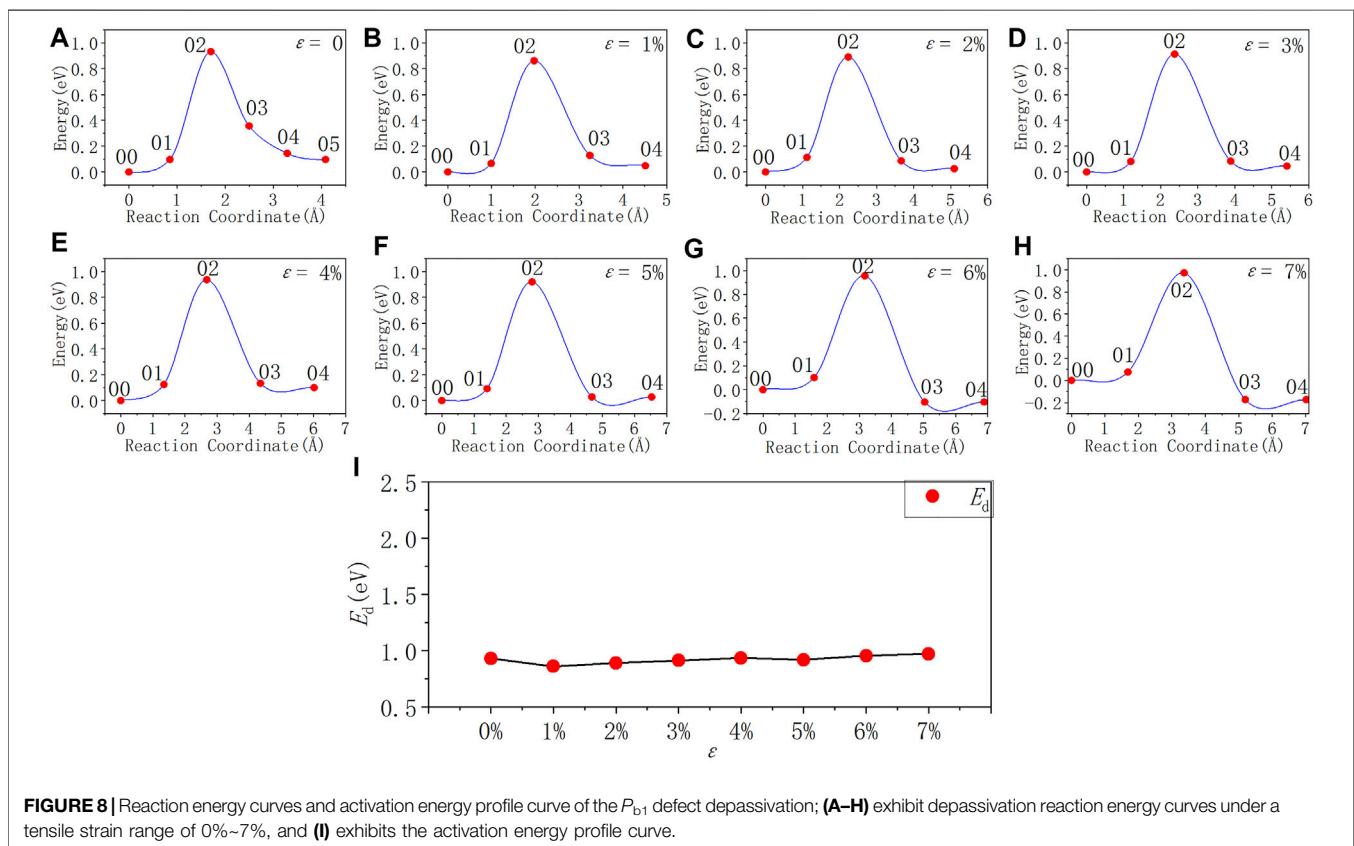


FIGURE 8 | Reaction energy curves and activation energy profile curve of the P_{b1} defect depassivation; (A–H) exhibit depassivation reaction energy curves under a tensile strain range of 0%–7%, and (I) exhibits the activation energy profile curve.

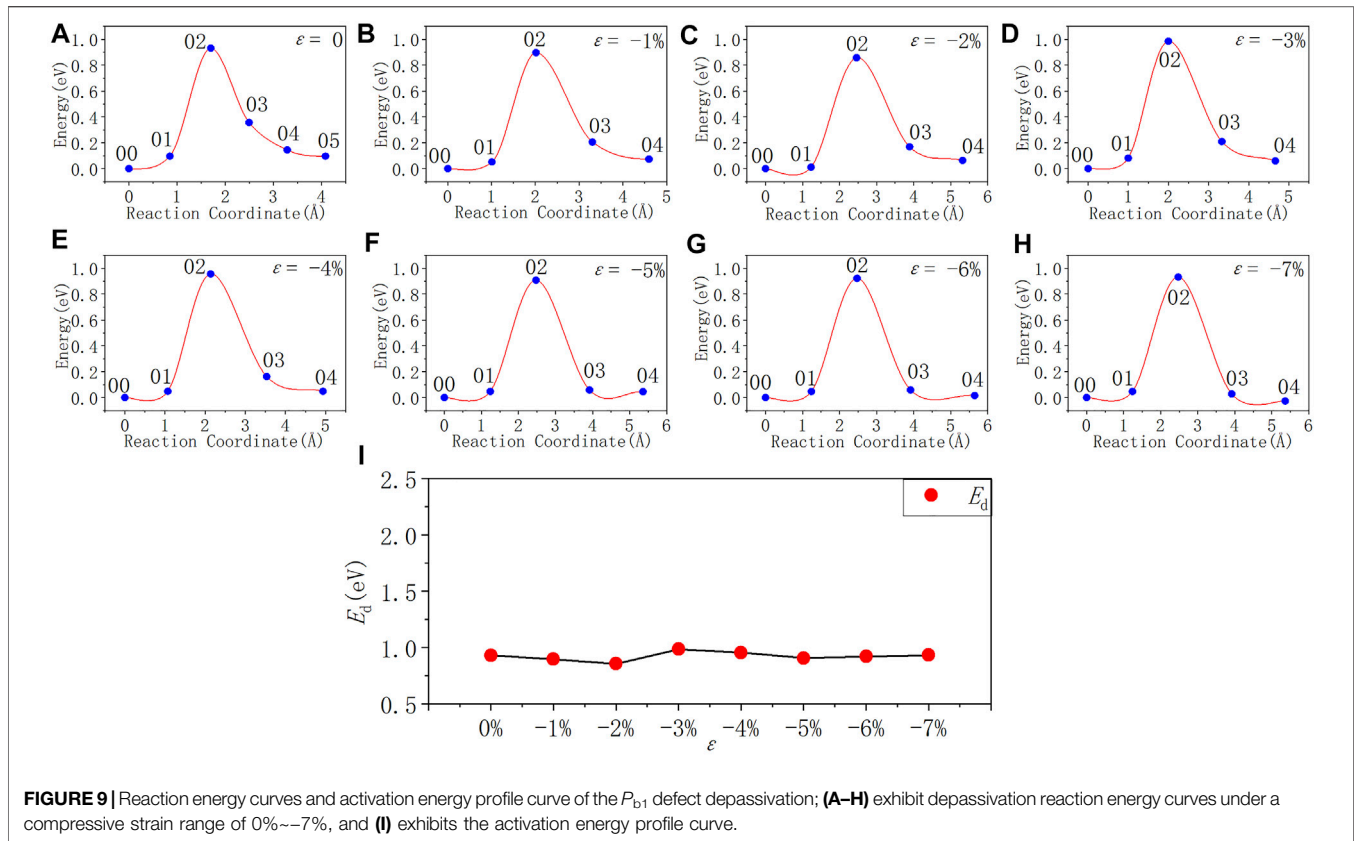


TABLE 9 | Depassivation reaction rates of P_b and P_{b1} defects under compressive strains at 300 K.

ε	0%	-1%	-2%	-3%
$K_d(P_b)/\text{cm}^3\text{s}^{-1}$	4.77×10^{-31}	4.65×10^{-32}	3.39×10^{-32}	4.82×10^{-32}
$K_d(P_{b1})/\text{cm}^3\text{s}^{-1}$	6.26×10^{-24}	2.55×10^{-23}	1.85×10^{-22}	1.85×10^{-24}
ε	-4%	-5%	-6%	-7%
$K_d(P_b)/\text{cm}^3\text{s}^{-1}$	3.01×10^{-27}	2.11×10^{-23}	9.69×10^{-21}	4.71×10^{-20}
$K_d(P_{b1})/\text{cm}^3\text{s}^{-1}$	6.89×10^{-24}	1.77×10^{-23}	1.37×10^{-23}	1.36×10^{-23}

TABLE 10 | Depassivation reaction rates of P_b and P_{b1} defects under tensile strains at 300 K.

ε	0%	1%	2%	3%
$K_d(P_b)/\text{cm}^3\text{s}^{-1}$	4.77×10^{-31}	1.64×10^{-31}	2.32×10^{-30}	2.40×10^{-30}
$K_d(P_{b1})/\text{cm}^3\text{s}^{-1}$	6.26×10^{-24}	9.23×10^{-23}	4.54×10^{-23}	2.43×10^{-23}
ε	4%	5%	6%	7%
$K_d(P_b)/\text{cm}^3\text{s}^{-1}$	6.09×10^{-30}	9.23×10^{-43}	1.38×10^{-41}	3.59×10^{-41}
$K_d(P_{b1})/\text{cm}^3\text{s}^{-1}$	7.87×10^{-24}	2.00×10^{-23}	5.30×10^{-24}	3.30×10^{-24}

respectively (Nickel et al., 1996). Based on the previous research $[H^+]$ in Eq. 5 is set to 10^{19} cm^{-3} in our work, and the relative concentration x_{P_b} and $x_{P_{b1}}$ of P_b and P_{b1} defects as a function of time are plotted in Figure 11.

It can be seen from Figure 11 that compared with the P_b defect, the depassivation of the P_{b1} defect is relatively insensitive to stress, which can be explained through their local structures.

For the P_{b1} defect, one of the three silicon atoms bonded to the defective atom is also bonded to three oxygen atoms, so the defective silicon atom is connected to the silicon substrate through a $[\cdot\text{Si}-\text{Si}(\text{O})_2-\text{Si}]$ structure, whereas the defective silicon atom of the P_b defect is directly connected to the silicon substrate through a $[\cdot\text{Si}-\text{Si}]$ structure. In a nutshell, the Si-O-Si bridge exists in the P_{b1} defect, but not in the P_b defect. The different depassivation performances for the two defects under stress are owing to the softness of the Si-O-Si bridge. Compared to the Si-Si-Si bond angle, the energy required to change the Si-O-Si bond angle is much lower, so the P_{b1} defect can release local stress through a torsion of its structure, therefore making itself insensitive to stress (Li et al., 2019b). However, the P_b defect is short of a structure like the Si-O-Si bridge, so it is more sensitive to the applied stress.

For $P_{b1}H$ defects at $a\text{-SiO}_2/\text{Si}(100)$ interface, it takes up to $10^3\text{--}10^6 \text{ s}$ to depassivate them with protons to P_{b1}^+ at room temperature, which is consistent with the experimental results summarized by Schwank et al. (2008) on the accumulation rate of interface traps. When the strain degree ε of the $a\text{-SiO}_2/\text{Si}(100)$ interface is -2%, 1% or 2% (equivalent to the interface pressure of about 1.36 GPa, -0.30 GPa or -0.80 GPa), the depassivation reaction rate of $P_{b1}H$ defects is the fastest. The total time for protons to depassivate all $P_{b1}H$ into P_{b1}^+ is about $10^3\text{--}10^4 \text{ s}$. When ε is -3%, 6% or 7% (equivalent to the interface pressure of about 1.78 GPa, -2.30 GPa or -2.60 GPa), the depassivation reaction rate of $P_{b1}H$ defects is the slowest. At this time, it takes about $10^5\text{--}10^6 \text{ s}$ for the $P_{b1}H$ depassivation reaction to reach saturation.

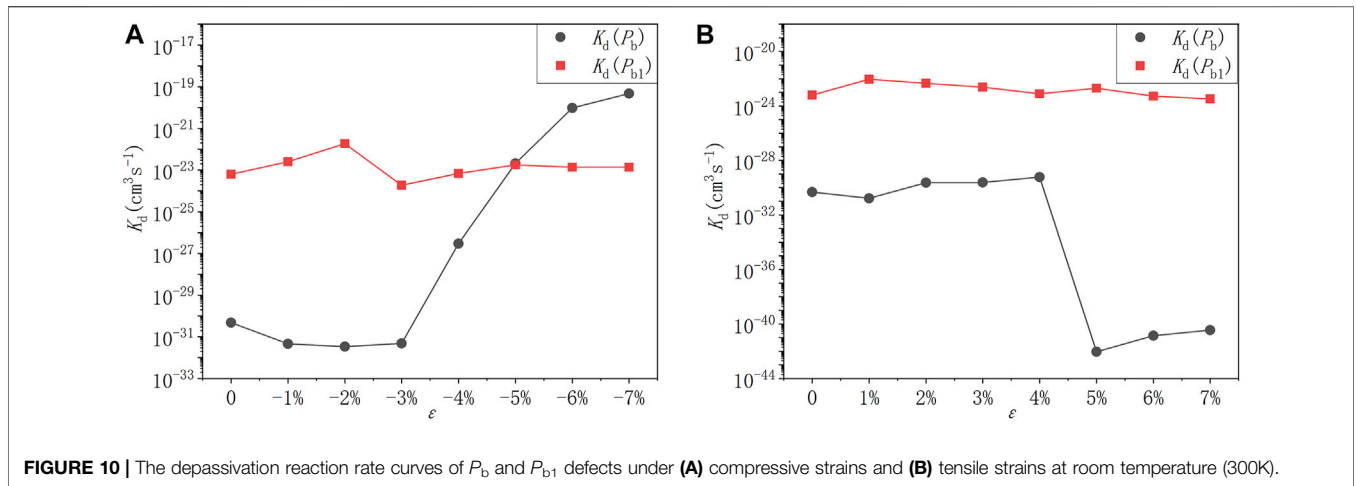


FIGURE 10 | The depassivation reaction rate curves of P_b and P_{b1} defects under (A) compressive strains and (B) tensile strains at room temperature (300K).

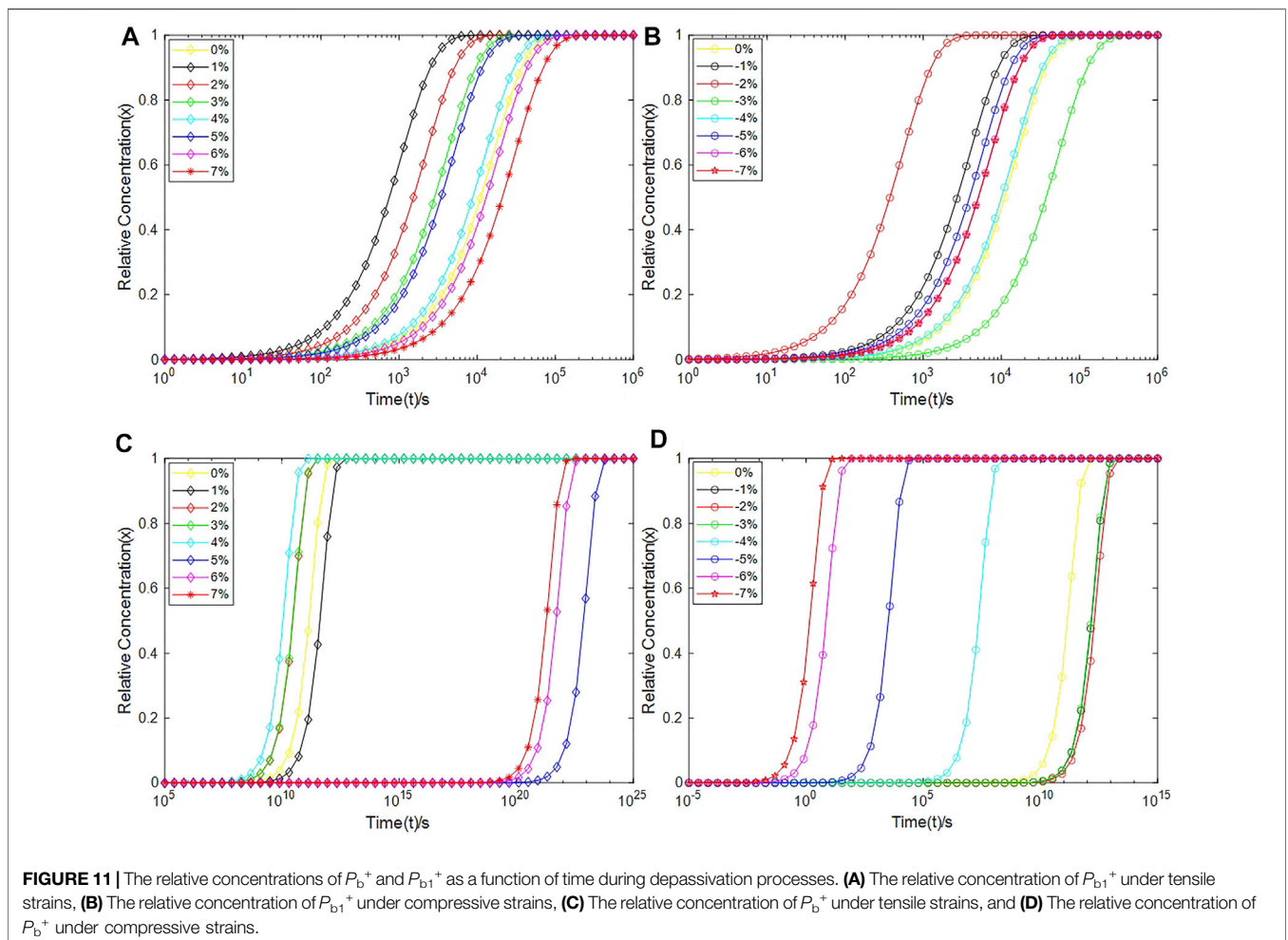


FIGURE 11 | The relative concentrations of P_b^+ and P_{b1}^+ as a function of time during depassivation processes. (A) The relative concentration of P_{b1}^+ under tensile strains, (B) The relative concentration of P_{b1}^+ under compressive strains, (C) The relative concentration of P_b^+ under tensile strains, and (D) The relative concentration of P_b^+ under compressive strains.

For $P_b\text{H}$ defects at $\alpha\text{-SiO}_2/\text{Si}$ (111) interface, stress greatly impacts the time taken for the depassivation reaction. When the strain degree ϵ of $\alpha\text{-SiO}_2/\text{Si}$ (111) interface is -5% , -6% or -7% (equivalent to the interface pressure of about 3.20, 3.50 or

3.90 GPa), the $P_b\text{H}$ depassivation reaction rate is relatively high, and all $P_b\text{H}$ depassivation reactions can reach saturation within 10^5 s, especially when ϵ is -6% or -7% , it takes only 10^2 s to depassivate all $P_b\text{H}$ into P_b^+ defects. When the strain degree ϵ of

a -SiO₂/Si (111) interface is 5%, 6%, 7% (equivalent to the interface pressure of about -1.90 , -2.30 GPa or -2.60 GPa), the P_b H depassivation reaction rate is very slow. In these cases, the time needed to depassivate all P_b H at the interface to P_b^+ is about 10^{23} – 10^{24} s.

CONCLUSION

The first-principles calculation method based on density functional theory is hired to investigate the impact of stress on the depassivation reaction of P_b defects at a -SiO₂/Si (111) interface and P_{b1} defects at a -SiO₂/Si (100) interface. In order to simulate the final passivation layer stress of the interfaces, biaxial strain is applied to the model, and stress-strain curves are plotted to verify the rationality of the stress application. Based on the kinetic theory of P_b -type defect proton depassivation, the equation of the relative concentration x of interface defects is derived. The HTST theory combined with the CI-NEB method is hired to calculate the depassivation reaction rate constant k_d . Finally, the relative concentration change curves of P_b defects and P_{b1} defects during depassivation under different stresses are illustrated.

It is shown that stress has an obvious impact on the depassivations of the P_b defect and the P_{b1} defect, as reflected in the reaction activation energy and reaction rate. By applying different degrees of stresses, the depassivation reaction rates of the P_b defect can be 10 orders of magnitude slower or faster than that under no stress, and the reaction time can be controlled from 10^1 to 10^{25} s. In contrast, the depassivation reaction of the P_{b1} defect is insensitive to the applied stress because of its local structure. Under different stresses, the depassivation reaction rates hardly show an excessive increase or decrease, and the depassivation reaction time is stably distributed in the range of 10^3 – 10^6 s, which is consistent with the experimental data given in

the literature. It has been shown that stress can impact radiation-induced charge buildup in MOS structures, and it is also responsible for the ELDRS (Chin and Ma, 1983; Zekeriya and Ma, 1984; Kasama et al., 1986; Shaneyfelt et al., 2002; Boch et al., 2003; Shaneyfelt et al., 2003). We show that the P_b defect is more sensitive to the applied stress, hinting that stress may be an effective way to control its properties. It could be predicted that the stress may impact the P_b defect and then influence ELDRS indirectly.

DATA AVAILABILITY STATEMENT

The raw data supporting the conclusion of this article will be made available by the authors, without undue reservation.

AUTHOR CONTRIBUTIONS

XZ and XL conceived the idea. XH-L performed the DFT calculations and data analysis. XL wrote the manuscript and XZ provided writing guidance. All authors discussed the results. XZ and YL supervised the execution of the whole work. All authors listed have made a substantial, direct and intellectual contribution to the work, and approved it for publication.

FUNDING

This research is supported by the Science Challenge Project (Grant No. TZ2016003-1-105), the Tianjin Natural Science Foundation (Grant No. 20JCZDJC00750), and the Fundamental Research Funds for the Central Universities–Nankai University (Grant No. 63211107 and 63201182).

REFERENCES

- Al-Shami, A., Lakhal, M., Hamedoun, M., El Kenz, A., Benyoussef, A., Loulidi, M., et al. (2018). Tuning the Optical and Electrical Properties of Orthorhombic Hybrid Perovskite CH₃NH₃PbI₃ by First-Principles Simulations: Strain-Engineering. *Solar Energ. Mater. Solar Cell.* 180, 266–270. doi:10.1016/j.solmat.2017.06.047
- Blöchl, P. E. (2000). First-principles Calculations of Defects in Oxygen-Deficient Silica Exposed to Hydrogen. *Phys. Rev. B* 62 (10), 6158–6179. doi:10.1103/physrevb.62.6158
- Blöchl, P. E. (1994). Projector Augmented-Wave Method. *Phys. Rev. B* 50 (24), 17953–17979. doi:10.1103/physrevb.50.17953
- Boch, J., Fleetwood, D. M., Schrimpf, R. D., Cizmarik, R. R., and Saigne, F. (2003). Impact of Mechanical Stress on Total-Dose Effects in Bipolar ICs. *IEEE Trans. Nucl. Sci.* 50, 2335–2340. doi:10.1109/tns.2003.820768
- Brower, K. L., and Myers, S. M. (1990). Chemical Kinetics of Hydrogen and (111) Si-SiO₂ interface Defects. *Appl. Phys. Lett.* 57 (2), 162–164. doi:10.1063/1.103971
- Chen, D. (2010). “The Effects of ELDRS at Ultra-low Dose Rates,” in 2010 IEEE Radiation Effects Data Workshop, 6. doi:10.1109/REDW.2010.5619506
- Chin, M. R., and Ma, T. P. (1983). Gate-width Dependence of Radiation-induced Interface Traps in metal/SiO₂/Si Devices. *Appl. Phys. Lett.* 42 (10), 883–885. doi:10.1063/1.93774
- Fogarty, J. C., Aktulga, H. M., Grama, A. Y., van Duin, A. C. T., and Pandit, S. A. (2010). A Reactive Molecular Dynamics Simulation of the Silica-Water Interface. *J. Chem. Phys.* 132, 174704. doi:10.1063/1.3407433
- Godet, J., and Pasquarello, A. (2006). Proton Diffusion Mechanism in AmorphousSiO₂. *Phys. Rev. Lett.* 97, 155901. doi:10.1103/physrevlett.97.155901
- Grote, C., and Berger, R. F. (2015). Strain Tuning of Tin-Halide and Lead-Halide Perovskites: A First-Principles Atomic and Electronic Structure Study. *J. Phys. Chem. C* 119, 22832–22837. doi:10.1021/acs.jpcc.5b07446
- Henkelman, G., Uberuaga, B. P., and Jónsson, H. (2000). A Climbing Image Nudged Elastic Band Method for Finding Saddle Points and Minimum Energy Paths. *J. Chem. Phys.* 113, 9901–9904. doi:10.1063/1.1329672
- Henry, E. (1935). The Activated Complex in Chemical Reactions. *J. Chem. Phys.* 3 (2), 107–115. doi:10.1063/1.1749604
- Hong, Z. C., and Zuo, X. (2020). Amorphous SiO₂/Si Interface Defects and Mechanism of Passivation/Depassivation Reaction. *J. Syst. Simulation* 32, 2362. doi:10.16182/j.issn1004731x.joss.20-FZ0474E
- HSteinfeld, J. I., Francisco, J. S., and Hase, W. L. (1999). *Chemical Kinetics and dynamics[M]*. Upper Saddle River, NJ: Prentice-Hall.
- Hughes, H. L., and Benedetto, J. M. (2003). Radiation Effects and Hardening of MOS Technology: Devices and Circuits. *IEEE Trans. Nucl. Sci.* 50 (3), 500–521. doi:10.1109/TNS.2003.812928
- Kasama, K., Toyokawa, F., Tsukiji, M., Sakamoto, M., and Kobayashi, K. (1986). Mechanical Stress Dependence of Radiation Effects in MOS

- Structures. *IEEE Trans. Nucl. Sci.* 33, 1210–1215. doi:10.1109/tns.1986.4334580
- Kovačević, G., and Pivac, B. (2014). Structure, Defects, and Strain in Silicon-Silicon Oxide Interfaces. *J. Appl. Phys.* 115 (4), 043531. doi:10.1063/1.4862809
- Kresse, G., and Furthmüller, J. (1996). Efficient Iterative Schemes For Ab Initio Total-Energy Calculations Using a Plane-Wave Basis Set. *Phys. Rev. B* 54, 11169–11186. doi:10.1103/physrevb.54.11169
- Lenahan, P. M. (2003). Atomic Scale Defects Involved in MOS Reliability Problems. *Microelectronic Eng.* 69 (2-4), 173–181. doi:10.1016/s0167-9317(03)00294-6
- Li, P., Song, Y., and Zuo, X. (2019a). Computational Study on Interfaces and Interface Defects of Amorphous Silica and Silicon. *Phys. Status Solidi RRL* 13, 1800547. doi:10.1002/pssr.201800547
- Li, P., Chen, Z., Yao, P., Zhang, F., Wang, J., Song, Y., et al. (2019b). First-Principles Study of Defects in Amorphous-SiO₂/Si Interfaces. *Appl. Surf. Sci.* 483, 231–240. doi:10.1016/j.apsusc.2019.03.216
- Li, P., Song, Y., and Zuo, X. (2018). Computational Study on Interfaces and Interface Defects of Amorphous Silica and Silicon. *Phys. Status Solidi RRL* 22, 1800547. doi:10.1002/pssr.201800547
- Mehes, E., and Patterson, C. H. (2017). Defects at the Si (001)/a-SiO₂ Interface: Analysis of Structures Generated with Classical Force Fields and Density Functional Theory. *Phys. Rev. Mater.* 1 (4), 044602. doi:10.1103/physrevmaterials.1.044602
- Nickel, N. H., Jackson, W. B., and Walker, J. (1996). Hydrogen Migration in Polycrystalline Silicon. *Phys. Rev. B* 53(12), 7750–7761. doi:10.1103/physrevb.53.7750
- Pease, R. L., Schrimpf, R. D., and Fleetwood, D. M. (2008). “ELDRS in Bipolar Linear Circuits: A Review,” in 2008 European Conference on Radiation and Its Effects on Components and Systems, 18–32. doi:10.1109/RADECS.2008.5782678
- Pei, G., Ying-Ying, Y., Wan-Duo, M., Xiao-Yong, F., Xi-Li, J., and Ya-Hui, J. (2021). Transport and Recombination Properties of Group-III Doped SiCNTs. *Physica E* 128, 114578. doi:10.1016/j.physe.2020.114578
- Perdew, J. P., Burke, K., and Ernzerhof, M. (1996). Generalized Gradient Approximation Made Simple. *Phys. Rev. Lett.* 77 (18), 3865–3868. doi:10.1103/physrevlett.77.3865
- Plimpton, S. (1995). Fast Parallel Algorithms for Short-Range Molecular Dynamics. *J. Comput. Phys.* 117, 1–19. doi:10.1006/jcph.1995.1039
- Poindexter, E. H., Caplan, P. J., Deal, B. E., and Razouk, R. R. (1981). Interface States and Electron Spin Resonance Centers in Thermally Oxidized (111) and (100) Silicon Wafers. *J. Appl. Phys.* 52 (2), 879–884. doi:10.1063/1.328771
- Rashkeev, S. N., Fleetwood, D. M., Schrimpf, R. D., and Pantelides, S. T. (2001). Defect Generation by Hydrogen at the Si-SiO₂ Interface. *Phys. Rev. Lett.* 87 (16), 165506. doi:10.1103/physrevlett.87.165506
- Schwank, J. R., Shaneyfelt, M. R., Fleetwood, D. M., Felix, J. A., Dodd, P. E., Paillet, P., et al. (2008). Radiation Effects in MOS Oxides. *IEEE Trans. Nucl. Sci.* 55 (4), 1833–1853. doi:10.1109/tns.2008.2001040
- Shaneyfelt, M. R., Pease, R. L., Maher, M. C., Schwank, J. R., Gupta, S., Dodd, P. E., et al. (2003). Passivation Layers for Reduced Total Dose Effects and ELDRS in Linear Bipolar Devices. *IEEE Trans. Nucl. Sci.* 50, 1784–1790. doi:10.1109/tns.2003.820771
- Shaneyfelt, M. R., Pease, R. L., Schwank, J. R., Maher, M. C., Hash, G. L., Fleetwood, D. M., et al. (2002). Impact of Passivation Layers on Enhanced Low-Dose-Rate Sensitivity and Pre-irradiation Elevated-Temperature Stress Effects in Bipolar Linear ICs. *IEEE Trans. Nucl. Sci.* 49 (6), 3171–3179. doi:10.1109/TNS.2002.805365
- Stathis, J. H., and Cartier, E. (1994). Atomic Hydrogen Reactions with Pb Centers at the (100) Si/SiO₂ Interface. *Phys. Rev. Lett.* 72 (17), 2745–2748. doi:10.1103/physrevlett.72.2745
- Stesmans, A., Nouwen, B., and Afanas'ev, V. V. (1998). P_bi Interface Defect in thermal(100)Si/SiO₂: ²⁹Si Hyperfine Interaction. *Phys. Rev. B* 58 (23), 15801–15809. doi:10.1103/physrevb.58.15801
- Stirling, A., Pasquarello, A., Charlier, J. C., and Car, R. (2000). Dangling Bond Defects at Si-SiO₂ Interfaces: Atomic Structure of the P_bi Center. *Phys. Rev. Lett.* 85 (13), 2773–2776. doi:10.1103/physrevlett.85.2773
- Stirling, A., and Pasquarello, A. (2005). Modelling of Paramagnetic Trivalent Silicon Defect Centres in Amorphous Silica and at Si-SiO₂ Interfaces. *J. Phys. Condens. Matter* 17 (21), S2099–S2113. doi:10.1088/0953-8984/17/21/006
- van Duin, A. C. T., Dasgupta, S., Lorant, F., and Goddard, W. A. (2001). ReaxFF: a Reactive Force Field for Hydrocarbons. *J. Phys. Chem. A* 105, 9396–9409. doi:10.1021/jp004368u
- van Duin, A. C. T., Strachan, A., Stewman, S., Zhang, Q., Xu, X., and Goddard, W. A. (2003). ReaxFFSiO Reactive Force Field for Silicon and Silicon Oxide Systems. *J. Phys. Chem. A* 107, 3803–3811. doi:10.1021/jp0276303
- Vineyard, G. H. (1957). Frequency Factors and Isotope Effects in Solid State Rate Processes. *J. Phys. Chem. Sol.* 3 (1-2), 121–127. doi:10.1016/0022-3697(57)90059-8
- Voter, A. F., and Doll, J. D. (1984). Transition State Theory Description of Surface Self-diffusion: Comparison with Classical Trajectory Results. *J. Chem. Phys.* 80 (11), 5832–5838. doi:10.1063/1.446610
- Witczak, S. C., Laco, R. C., Osborn, J. V., Hutson, J. M., and Moss, S. C. (2005). Dose-Rate Sensitivity of Modern nMOSFETs. *IEEE Trans. Nucl. Sci.* 52 (6), 2602–2608. doi:10.1109/tns.2005.860709
- Ya-Hui, J., Pei, G., Shu-Long, L., Wan-Duo, M., Xiao-Yong, F., Ying-Ying, Y., et al. (2020). Effects of Hydroxyl Groups and Hydrogen Passivation on the Structure, Electrical and Optical Properties of Silicon Carbide Nanowires. *Phys. Lett. A* 384, 126106. doi:10.1016/j.physleta.2019.126106
- Ying-Ying, Y., Pei, G., Wan-Duo, M., Rui, H., and Xiao-Yong, F. (2021). Effects of Substitution of Group-V Atoms for Carbon or Silicon Atoms on Optical Properties of Silicon Carbide Nanotubes*. *Chin. Phys. B* 30, 067803. doi:10.1088/1674-1056/abdb1e
- Yue, Y., Wang, J., Zhang, Y., Song, Y., and Zuo, X. (2018). Interactions of Atomic Hydrogen with Amorphous SiO₂. *Physica B: Condensed Matter* 533, 5–11. doi:10.1016/j.physb.2017.12.056
- Zekeriya, V., and Ma, T.-P. (1984). Dependence of X-ray Generation of Interface Traps on Gate Metal Induced Interfacial Stress in MOS Structures. *IEEE Trans. Nucl. Sci.* 31, 1261–1266. doi:10.1109/tns.1984.4333493
- Zhou, W., Liu, Y., Yang, Y., and Wu, P. (2014). Band Gap Engineering of SnO₂ by Epitaxial Strain: Experimental and Theoretical Investigations. *J. Phys. Chem. C* 118, 6448–6453. doi:10.1021/jp500546r

Conflict of Interest: The authors declare that the research was conducted in the absence of any commercial or financial relationships that could be construed as a potential conflict of interest.

Publisher's Note: All claims expressed in this article are solely those of the authors and do not necessarily represent those of their affiliated organizations or those of the publisher, the editors, and the reviewers. Any product that may be evaluated in this article, or claim that may be made by its manufacturer, is not guaranteed or endorsed by the publisher.

Copyright © 2022 Liu, Liu, Zhu, Liu, Zhang and Zuo. This is an open-access article distributed under the terms of the Creative Commons Attribution License (CC BY). The use, distribution or reproduction in other forums is permitted, provided the original author(s) and the copyright owner(s) are credited and that the original publication in this journal is cited, in accordance with accepted academic practice. No use, distribution or reproduction is permitted which does not comply with these terms.